

Simulation of Fracture Healing in the Tibia: Mechanoregulation of Cell Activity Using a Lattice Modeling Approach

Damien P. Byrne,¹ Damien Lacroix,² Patrick J. Prendergast¹

¹Trinity Centre for Bioengineering, School of Engineering, Parsons Building, Trinity College, Dublin 2, Ireland, ²Institute for Bioengineering of Catalonia, Barcelona, Spain

Received 10 September 2009; accepted 28 December 2010

Published online 1 April 2011 in Wiley Online Library (wileyonlinelibrary.com). DOI 10.1002/jor.21362

ABSTRACT: In this study, a three-dimensional (3D) computational simulation of bone regeneration was performed in a human tibia under realistic muscle loading. The simulation was achieved using a discrete lattice modeling approach combined with a mechanoregulation algorithm to describe the cellular processes involved in the healing process—namely proliferation, migration, apoptosis, and differentiation of cells. The main phases of fracture healing were predicted by the simulation, including the bone resorption phase, and there was a qualitative agreement between the temporal changes in interfragmentary strain and bending stiffness by comparison to experimental data and clinical results. Bone healing was simulated beyond the reparative phase by modeling the transition of woven bone into lamellar bone. Because the simulation has been shown to work with realistic anatomical 3D geometry and muscle loading, it demonstrates the potential of simulation tools for patient-specific pre-operative treatment planning. © 2011 Orthopaedic Research Society. Published by Wiley Periodicals, Inc. *J Orthop Res* 29:1496–1503, 2011

Keywords: fracture healing; lattice modeling; mechanoregulation; computational simulation; anatomical data

The loading on the regenerate tissue during fracture healing is determined by both the method of fixation and the physical activity of the patient. Determining the appropriate biomechanical treatment to promote optimal bone regeneration during fracture healing remains the subject of much research. Mechanobiology may prove useful in determining optimal treatments as it is concerned with the mechanism by which biological processes are regulated by signals to cells that are induced by mechanical loads.^{1,2} Continuum theories describing the relationship between mechanical stimuli and tissue phenotype were originally proposed in relation to fracture healing. These theories were later formulated algorithmically for numerical solution. Computational simulations to predict tissue regeneration combine finite element modeling (to compute the mechanical stimuli in the tissues), and mechanoregulation algorithms (to adapt the tissue material properties in iterative computational schemes). Isaksson et al.³ compared the different mechanoregulation theories proposed by Carter et al.,⁴ Claes and Heigle,⁵ and Prendergast et al.⁶ and found that the tissue differentiation patterns predicted by the combined biophysical stimuli of deviatoric strain and fluid velocity was closest to experimental results. The theory based on strain and fluid flow stimuli was the only one able to predict healing under torsional loading as seen *in vivo*. This approach has been successfully employed by others to predict tissue differentiation patterns in many areas of bone healing, such as osseointegration around implants,⁷ fracture healing,^{8–10} osteochondral defect healing,¹¹ regeneration of an osteotomized mandible,¹² and also

to analyze tissue differentiation inside bone chambers.^{13,14}

Until recently many simulations used diffusion to model cellular activity within the regenerating tissue.^{7,8,11–13} However, this approach implicitly assumes that cells attempt to achieve a homogenous population density within the area of analysis. Isaksson et al.¹⁵ recently combined the mechanoregulation algorithm of Prendergast et al.⁶ with a set of coupled nonlinear differential equations to describe transport/migration, proliferation, differentiation, and apoptosis of cells. They used a two-dimensional (2D) finite element model of a long bone osteotomy to evaluate the model's potential and found that the cell phenotype-specific processes are very important to take into account, as they largely determine the outcome of the stimulations. Pérez and Prendergast¹⁶ proposed an alternative approach to diffusion—namely a “random-walk” of cells within a lattice to model proliferation and migration. This approach facilitates easy modeling of the simultaneous dispersal of different cell phenotypes, the explicit modeling of cell proliferation, apoptosis by adding/removing cells from lattice points, and, more generally, the possibility of implementing complex cell-based rules for cell activities.

The objective of this work is to model fracture healing in a human tibia using the lattice approach to account explicitly for cell activity. Specifically, we hypothesize that computational simulations of fracture healing in the tibia under realistic muscle loading and with an external fixator applied, can predict healing similar to that found *in vivo*. The study has the objective of simulating fracture healing beyond the reparative phase into the resorption phase for realistic anatomical fractures. If this approach proves feasible it offers the possibility of using computer simulations in the clinical treatment of complex fractures, and in other orthopedic applications where bone regeneration occurs.

Additional Supporting Information may be found in the online version of this article.

Correspondence to: Patrick J. Prendergast (T: +353-1-608-1383; F: +353-1-679-5554. E-mail: pprender@tcd.ie)

© 2011 Orthopaedic Research Society. Published by Wiley Periodicals, Inc.

METHODS

Mechanoregulation and Cellular Activity

Tissue differentiation is regulated by magnitudes of shear strain (γ) and relative fluid/solid velocity (v) in the extracellular matrix, according to the equation: $S = \gamma/a + v/b$, where $a = 0.0375$ and $b = 3 \mu\text{ms}^{-1}$; Huiskes et al.¹⁷ used these values to successfully predict the patterns of tissue differentiation observed experimentally by Søballe et al.¹⁸ Shear strain and fluid velocity are calculated from a biphasic poroelastic finite element analysis, and, depending on the value of S , a tissue phenotype is predicted—high stimulus levels promote the differentiation of mesenchymal cells into fibroblasts, intermediate levels stimulate the differentiation into chondrocytes, low levels of these stimuli promote the differentiation into osteoblasts and very low values promote the activity of osteoclasts and resorption. The boundary values for shear strain and fluid velocity were taken from Lacroix and Prendergast¹⁹ which were corroborated by Isaksson et al.³ against the fracture healing histology of Claes and Heigle⁵ (inset to Figure 1).

The initial callus was assumed to consist of granulation tissue, into which mesenchymal stem cells (MSCs) could migrate and proliferate. The precursor cells originate from the periosteum, endosteum, and marrow space at the site of the damaged cortical bone tissue.²⁰ The random-walk approach is used to model the dispersal of the various cell populations in three-dimensions (3D) using a global “lattice.” The size and density of the global lattice is determined from the dimensions of the fracture callus and the distance between each lattice point (taken here as 0.08 mm). Each lattice point is considered a region of space where both a cell and the extracellular matrix may be located. Proliferation and migration is modeled on an unbiased nearest-neighbour random walk approach. It has been reported that the rate of cell division is regulated by mechanical stimuli as shown by, for example McMahon et al.²¹; therefore proliferation of the differentiated cell phenotypes was assumed to only occur in the appropriate mechanical stimuli field. Other factors such as oxygen tension²² and growth factors²³ which are not explicitly modeled in these simulations affect the rate of proliferation. Recognizing that migration is a

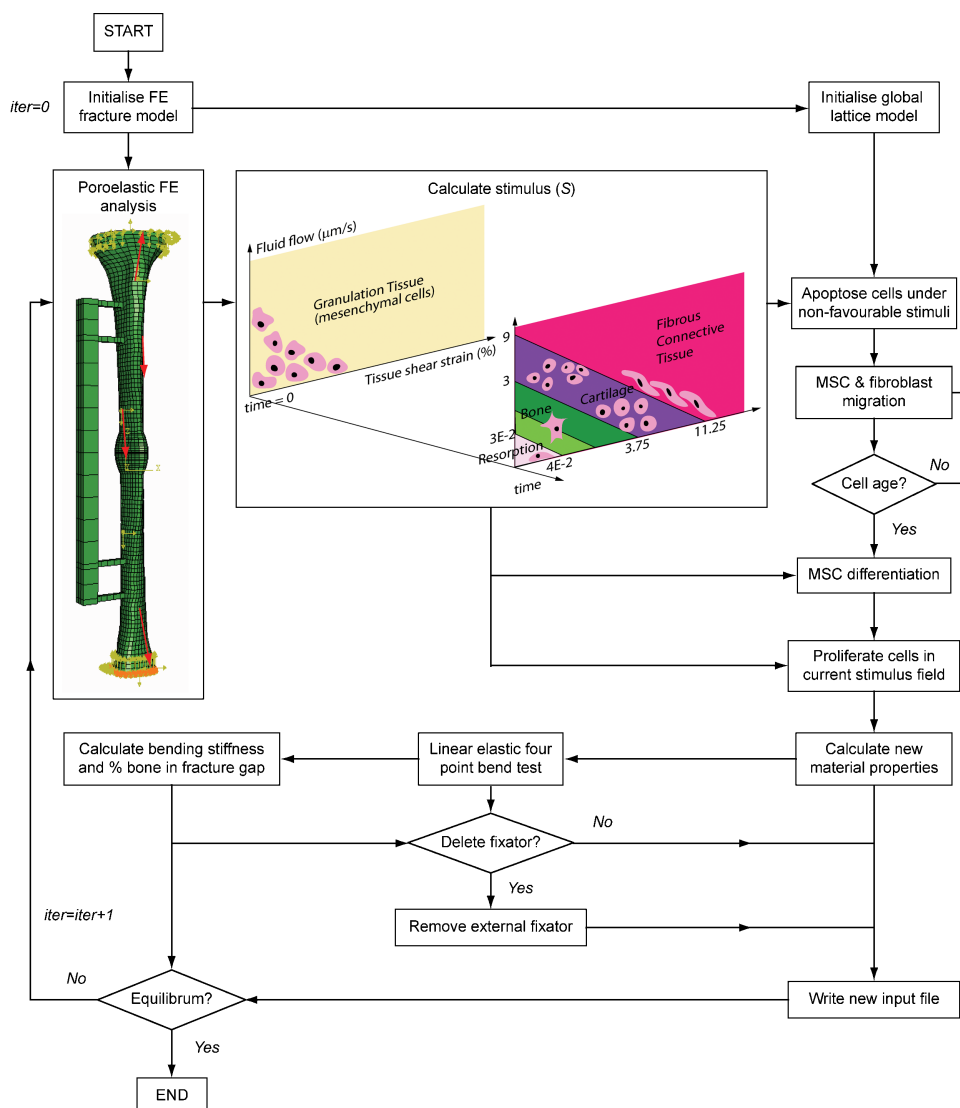


Figure 1. Flow chart of iterative computational simulation. The mechano-regulation diagram and finite element model (with boundary and loading conditions) are illustrated inset to their respective panels. The components of muscle and joint contact forces and coordinates of attachment points on the surface of the tibia are available as part of an electronic supplement.

Table 1. Cell Parameter Data (Per Day Unless Otherwise Stated)

	MSCs	Fibroblasts	Chondrocytes	Osteoblasts
Differentiation rate	0.3 ^{14,15}	—	—	—
Critical age	>6 days	—	—	—
Proliferation rate	0.5	0.3	0.3	0.3 ¹⁵
Migration rate	30 $\mu\text{m}/\text{h}$ ⁴¹	30 $\mu\text{m}/\text{h}$ ⁴¹	—	—
Maturation time	—	—	16 days ^{15,43}	30 days
Apoptosis rate	—	0.15	0.15	0.15 ¹⁵
Resorption rate	—	—	—	0.15

more rapid process than proliferation, a new location for a migrating cell is chosen n times per iteration of the proliferation process, with each iteration representing 48 h. As MSCs and fibroblasts are more motile during tissue repair than other cell populations, only these cell types are allowed to migrate in the model. This relates to a migration rate of 30 $\mu\text{m}/\text{h}$ (meaning n as defined above is equal to 9) in accordance with Saltzman.²⁴ Other cells disperse by proliferation only (Table 1).

The number of cells that differentiate in the lattice is established by multiplying the differentiation rate by the number of MSCs that have reached the critical age (Table 1). Once a cell has been stimulated down a particular lineage the differentiated cell requires time to synthesize and remodel new tissue. To describe the variation of the Young's modulus at a lattice point a rate equation is used.¹² The shape of the curve is set so that the Young's modulus of tissue phenotype (either fibrous tissue, cartilage, immature, or mature bone) increases in 30 days from the initial value of 0.2 MPa, typical of granulation tissue to the final values reported in Table 2. As time is based on the age of the cell, the start time for the rate equation is set locally after the deposition of a certain tissue type. The mechanoregulation algorithm is capable of predicting differentiation of cells into immature or mature woven bone, both of which are intermediate stages in bone repair. As healing progresses woven bone is gradually replaced by secondary lamellar bone.²⁵ Once the rate equation is complete it is necessary to model this transition. Therefore, if the mechanoregulation stimulus persists in a woven bone field the material properties (Young's modulus and permeability) are updated over time—such that immature woven bone evolves into mature woven bone over 60 days; while mature woven bone slowly transforms into cortical bone over 400 days.

In this study, apoptosis of the differentiated cell phenotypes was assumed to only occur outside that cell phenotypes'

biophysical stimulus field. Therefore, cells subject to a stimulus outside their field will begin to apoptose over time, based on a cell death rate of 15% per day. The cells chosen to apoptose are randomly selected in each element.

Finite Element Model

The same 3D geometry of a human left tibia as used by Lacroix and Prendergast⁸ was employed to model bone healing. A fracture gap of 3 mm was simulated with a homogeneous external callus with a callus index of 1.4. A unilateral external fixator with two pins was modeled and inserted in the anterior-medial side of the tibia (inset to Figure 1).

The cortical bone and external fixator were modeled as linear elastic materials, while all other tissues were modeled as biphasic poroelastic materials (Table 2). As cells at each lattice point differentiate based on the mechanoregulation stimuli, and each finite element contains many hundreds of lattice points, it is likely that several tissues will coexist within one element; therefore, the mechanical properties are averaged at the element level using the rule of mixtures. Thus the Young's modulus for every element is determined by the rate equation and a simple rule of mixtures. The rate equation was not used to determine the bulk modulus, permeability and Poisson's ratio of the granulation elements as there is no evidence to suggest that these mechanical properties increase exponentially with time. Similar to Lacroix et al. the material properties of an element were calculated as an average of the 10 previously predicted tissue phenotypes. Therefore, the required stimulus must be maintained for 10 iterations before the new tissue phenotype is formed within the element.^{19,26}

Regarding the permeability of bone, reported values used in previous mechanoregulatory simulations were based on well-organized trabecular bone free of marrow. The permeability of woven bone tissue is not known; however, it is likely that *in vivo*

Table 2. Material Properties of Tissue Phenotypes

	Young's Modulus (MPa)	Poisson's Ratio	Permeability ($\text{m}^4/\text{Ns} \times 10^{-14}$)	Porosity	Bulk modulus grain (MPa)
Granulation	0.2	0.167	1	0.8	2,300
Fibrous	2	0.167	1	0.8	2,300
Marrow	2	0.167	1	0.8	2,300
Cartilage	10	0.167	0.5	0.8	3,400
Immature	1,000	0.3	10	0.8	13,920
Mature	6,000	0.3	1.02	0.8	13,920
Cortical	17,000	0.3	—	—	—
Fixator	200,000	0.3	—	—	—

permeabilities would be lower due to the presence of soft tissue within the pores. Consequently, a lower permeability value of $1.02 \times 10^{-14} \text{ m}^4/\text{Ns}$ was used in this study.

The muscle and joint forces acting on the tibia were adapted from Duda et al.,²⁷ for the second peak in ground reactions during gait (45% of gait cycle). A body weight of 80 kg was assumed and only those muscles attaching to the tibia were included as single straight lines and made to match appropriate node co-ordinates. Following Duda et al.,²⁸ the total knee load was split 60–40% on the medial and lateral sides, respectively. In order to restrict rigid-body motions the nodes at the base of the model and 2 nodes on the external fixator were restrained in the transverse plane. The physiological loading conditions acting on a fractured human tibia with an external fixator are not precisely known. The simulation begins after the fracture callus has formed, by which time the patient should resume cautious load-bearing.²⁹ The loading acting on the tibia will vary depending on a number of factors such as, the severity of the fracture, fixation method used, the patient's age, weight, height, fitness, bone quality, etc.; therefore, the loading profile and hence the healing time line is patient specific. In this study, the loading profile is based on the general shape of the weight-bearing achieved by patients on their fractured leg; the healing period, however, was estimated due to the variation observed among patients in previous experimental studies.^{30–32} Therefore, following an initial rest period in which the callus was formed, it was assumed that the joint and muscle loads were increased from 10% to 20% over the first 48 days, thereafter they were ramped up to 100% over the following 126 days.

Iterative Simulation

The simulation begins with a poroelastic finite element analysis of the fractured tibia with an external fixator, using Abaqus v 6.5-1 (Hibbit, Karlsson and Sorensen, Inc., 2005). The tissue shear strain and relative fluid velocity are calculated and a tissue phenotype is predicted for each callus element according to the mechanoregulation algorithm. The cellular processes of the tissue phenotypes in each element are regulated by the resulting stimulus such that (a) MSCs differentiate into cell type i , based on the differentiation rate and the number of MSCs that have reached the critical age, (b) 60% of cell type i proliferate, and (c) cell types not under the current stimulus apoptose, based on the cell death rate (Table 1).

Cells are chosen randomly in each element. If the stimulus enters the resorption field the osteoblasts within that finite element are deleted from the lattice. Fully resorbed elements however, are deleted from the finite element mesh (apart from elements in the medullary cavity, which are assigned marrow material properties). The material properties of each element in the callus will evolve according to a combination of the rule of mixtures and the rate equation. These resulting material properties are then applied to a new simulation and the process is repeated, as illustrated in the flow chart in Figure 1.

To predict the evolution of bending stiffness during healing, a four-point bend test in the sagittal plane was also simulated at every stage of tissue differentiation. Deflection of the bone was calculated using linear elastic properties of the predicted tissue phenotypes. A bending stiffness was defined as the bending moment divided by the angle of deflection. According to Richardson et al.,³³ a stiffness of 15 Nm/degree provides a definition of union in tibial fractures. The external fixator was therefore removed when the stiffness exceeded this value.

The analysis continues until convergence of the bending stiffness has been achieved.

RESULTS

Once the infiltrating progenitor cells reached the critical age, tissue differentiation initiates automatically. Cartilaginous tissue and small amounts of fibrous tissue were predicted to form first between the bone ends (day 20 in Figure 2), while intramembranous ossification occurred along the surface of the tibial cortical bone outside the fracture gap. Bone formation persisted in the external callus through intramembranous ossification, while cartilage was gradually replaced by bone through endochondral ossification in the medullary cavity (day 40). This trend continued until the majority of the fracture callus became ossified (days 40–120). A small region of cartilage tissue remained at the posterior side of the fracture gap and external callus. At this time, osseous bridging became complete at the periphery of the callus, which effectively shielded the softer tissues of the callus from high mechanical stimuli. This effect then facilitated replacement of soft tissues with bone, until complete differentiation into bone in the external callus was achieved (day 120). Applying the criterion outlined in

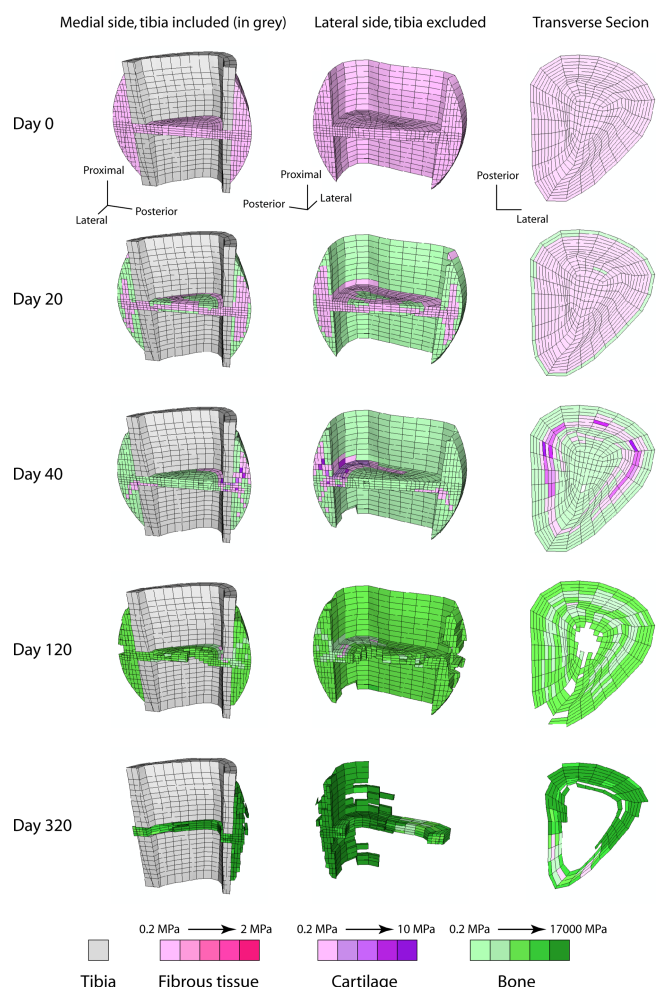


Figure 2. Cross-sectional view of the predicted healing patterns over time.

the Materials and Methods Section, the external fixator was automatically removed in day 122. The stability of the callus allowed resorption to take place in regions distal to the fracture gap and in the medullary cavity. From this point on, the remodeling process caused further resorption (days 120–320).

Bending occurred in the sagittal plane (posterior–anterior plane) which created greater mechanical stimuli in the posterior region of the fracture gap. Consequently, in order to support the greater loads, an amount of bone tissue remains in the intramedullary cavity and the posterior region of the external callus in the simulation (Figure 2, day 120). On the other hand, elements in the anterior gap experienced reduced mechanical stimuli causing some resorption. One or two elements in the anterior region of the interfragmentary gap “flipped” between the cartilage and bone fields, however, this was uncommon and was probably due to a localized numerical instability.

Looking in more detail at the biophysical stimuli during bone regeneration, the initial fluid flow and octahedral shear strain were generally high (Figure 3). Tissue differentiation caused an increase in stiffness of the callus and correspondingly less displacement, causing the biophysical stimuli to change. Then the biophysical stimuli in the elements began to move across the phenotype fields from fibrous tissue, cartilaginous tissue, and immature bone (days 20–40 in Figure 3). Over the following 80 days fluid decreased while octahedral shear strain increased, causing the majority of elements to fall into the mature bone field. Thereafter

the mechanical properties of the bone tissue were altered by modeling the transition of woven bone into lamellar bone. At the end of the simulation, the majority of elements in the fracture gap lie in the mature bone field.

The interfragmentary strain (IFS) was defined as the interfragmentary displacement divided by the initial fracture gap size. As the tibia experienced bending in the mid-diaphysis the IFS was calculated at four points in the fracture gap (anterior, posterior, medial, and lateral). The greatest of these values is plotted in Figure 4. The IFS initially increased as the progenitor cells had not reached the critical age for differentiation and the applied loading conditions increased over time. The strain then rapidly reduced over the following 6 weeks due to differentiation and maturation of the granulation tissue throughout the callus. Thereafter bony bridging occurred in the external callus, and the strain gradually reduced further due to the adaptation of the bone tissue. Finally, the IFS becomes very small after week 17, at which point the external and endosteal calluses began to resorb.

When the fracture callus consists entirely of granulation tissue the bending stiffness is very low (0.38 Nm/degree). As healing progressed, the bending stiffness increases rapidly within the first 6 weeks (Figure 5). The bending stiffness continues to increase gradually to reach a maximum value of 81 Nm/degree at week 24. This reduces slightly with resorption of the external callus and the intramedullary cavity, a phenomenon which can also be seen in the experimental results. Equilibrium is reached at a stiffness of 73 Nm/degree.

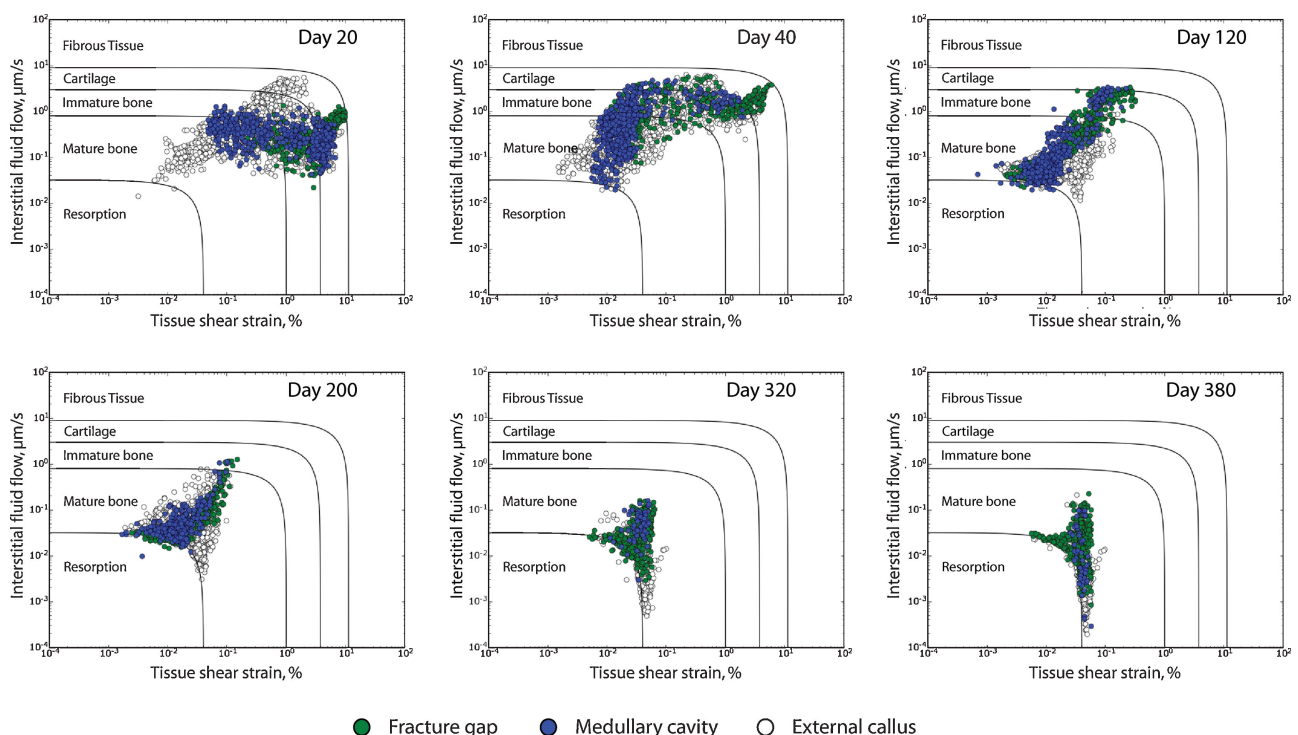


Figure 3. Mechano-regulation diagrams illustrating the interstitial fluid velocity and tissue shear strain at 20, 40, 120, 200, 320 and 380 days. The resorbed elements were deleted.

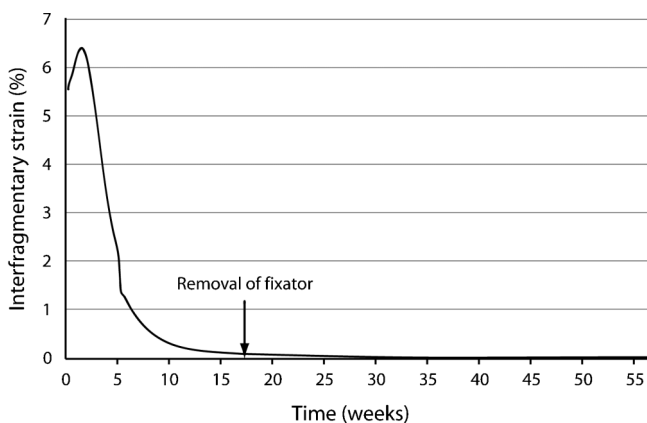


Figure 4. Interfragmentary strain decreases as healing occurs.

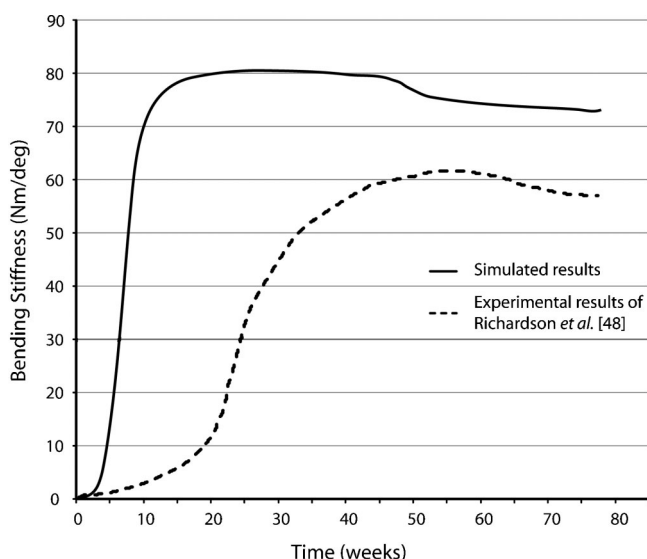


Figure 5. Comparison of the simulated bending stiffness against the experimental results of Richardson et al.³³

DISCUSSION

The objective of simulating fracture healing in an anatomically realistic tibia with muscle loading and with a fixator was achieved. The simulation successfully predicted the sequence of tissue differentiation patterns that appear in the callus; and healing was simulated beyond the reparative phase into the resorption phase. While the simulations of fracture healing have been presented by others,^{3,8–10,13,15,19,26,34–36} this work shows, in addition, that the inclusion of realistic muscle forces gives a simulation that continues into the resorption phase. Ultimately, a resorbed callus and a fully healed long bone is simulated. This conclusion that resorption is only possible when anatomical muscle loads act demonstrates that the simulation is sensitive to the loading conditions. The relative sophistication of the model in regard to bone geometry, as well as the explicit inclusion of cell activities using a lattice, opens up the possibility of further developing such simulations to aid in deciding on

clinical treatments of complex fractures on a patient-specific basis.

One limitation to the modeling approach presented is the difficulty in defining cell parameters. Isaksson et al.¹⁵ carried out an extensive review of the cellular rates used in mechanobiology models. Where appropriate these values were applied in this work; however, some parameters are not well defined in the literature and were standardized—this has led to some differences between the parameters used in this study and those used by Khayyeri et al.¹⁴ Once further information on cell activity rates becomes available it can easily be implemented into the lattice model. In particular, the differentiation rate and apoptosis rate must be more closely defined, as the balance between these processes determines the activities of the cell populations at any given time. Isaksson et al.¹⁵ also highlighted that the importance of the assumed cellular rates in the computational simulations are difficult to evaluate and an extensive parametric study is necessary to evaluate the importance of each assumption and its influence on the bone regeneration process.¹⁵ In vitro cellular experiments (cells in culture or single cells) involving mechanical stimulation could be used to determine the appropriate parameters for the mechanobiological models. For example, Kearney et al.³⁷ reported that cyclic uniaxial mechanical strain applied to MSCs seeded on a 2D silicone membrane, at magnitudes greater than 7.5%, induces apoptosis. Using a 3D collagen-GAG scaffold McMahon et al.²¹ also demonstrated that mechanical constraint (created by uniaxial clamping) and 10% cyclic tensile loading modulated the chondrogenic differentiation of MSCs. Furthermore, Weyts et al.³⁸ demonstrated that the response of osteoblasts to mechanical stresses vary with their state of differentiation in 7-day osteoblast cultures, tensile strain levels (0.4–2.5%) trigger apoptosis, whereas in more mature cultures apoptosis is not affected by the same treatment. Additionally, they found that stretching differentiating osteoblast cultures at day 14 increases proliferation. While the magnitude of the strain experienced by the cells in these studies is somewhat diminished from that which is applied to the substrate,³⁹ the results show that apoptosis threshold limits are not only cell-specific, but also dependent on the state of differentiation. This further emphasizes the importance of modeling the evolution of differentiating tissues by exclusively accounting for cell age in mechanoregulatory simulations. Limitations relating to the finite element model itself include the assumption that the simulation began after the inflammation phase of healing, and the entire callus consisted of granulation tissue into which MSCs could migrate and proliferate. The callus index was pre-defined with a value of 1.4, and, therefore, the model does not take callus growth into account. In addition, the material properties of the regenerating tissues have not yet been measured directly. Based on the work of Lacroix et al.¹⁹ the mechanical properties of the tissues were taken from the literature.

The simulations gave tissue differentiation patterns which agree with those observed histologically—namely (a) intramembranous ossification distal to the fracture site, (b) the gradual replacement of cartilage in the external and endosteal calluses through endochondral ossification, and finally (c) resorption of the external and endosteal calluses. Previous simulations did not successfully predict internal callus resorption.⁸ The progress of healing is also reflected in the predicted IFS and bending stiffness results. The initial range of moderate strains (6–10%) are similar to those observed by Gómez-Benito et al.,³⁴ while there was a qualitative agreement between predicted changes of IFS over time and experimental results.^{31,40} The general shape of the bending stiffness curve also corresponds to the experimental results of Richardson et al.³³; however, a time difference was observed and the numerical results exceed the normal bending stiffness of an intact tibia (approximately 60 Nm/degree). This may be attributed to the rates of the cellular processes used, or the fact that isotropic material properties were used in the finite element model.

It should be noted that the cellular processes used in the model did not operate independently of each other. Modeling of cell-scale properties such as MSC and fibroblast migration was more accurately defined using the lattice approach. The inclusion of migration has a direct effect on proliferation as it lowers the possibility of contact inhibition until confluence is achieved. Cell migration therefore contributes to higher proliferation rates and is essential when modeling cellular activity. The rates of cell motility were taken from the literature,^{15,24,41} and, therefore, no definitive time line for complete cell coverage was specified in the simulations. In turn, the number of cells that differentiate in the lattice was established by multiplying the differentiation rate by the number of MSCs that have reached the critical age. Therefore, the differentiation rate was dependent on the amount of cells available (which was regulated by the critical age, and the proliferation and migration rates of all the cellular phenotypes) and the mechanobiology stimulus.

One key attribute of the approach used is the explicit modeling of cell age, which enhances the possibility of accurately defining evolving material properties in relation to cell age and phenotype. It was assumed that MSC differentiation only occurred once the cells had reached a critical age, independent of the mechanical stimulus. Thereafter a maturation time was used to regulate the synthesis and remodeling of new osteogenic and cartilage tissue. Isaksson et al.¹⁵ highlighted that once a MSC has been stimulated down the osteogenic pathway, it proliferates 8–10 times before it matures and produces bone matrix⁴²; while chondrocytes may require up to 3 weeks to mature.⁴³ Describing the temporal change of the differentiating tissue in this manner gives a more accurate representation of the new material stiffness. Additionally, an attempt was made to model bone adaptation by increasing the

Young's modulus and decreasing the permeability of the woven bone tissue if the mechanoregulation stimulus remained low. By modeling the transition of woven bone into secondary lamellar bone, fracture healing was simulated beyond the reparative phase.

Another feature of this study is the application of a realistic 3D anatomical loading profile. However, the loading profile was based on the general shape of weight-bearing achieved by patients on their fractured leg. While the joint forces acting on the tibia may be correlated to the percentage of weight-bearing, it is questionable how much force the muscles exert in the initial stages of healing, particularly if they are inhibited by the presence of the external fixator. In the absence of more detailed information this method was assumed the most accurate way of representing the loading conditions.

In this study, we set out to show that fracture healing could be simulated in 3D, in a long bone subjected to realistic muscle loading. The simulation based on combining mechanoregulation of cell activities in a lattice with finite element modeling successfully predicted the sequence of tissue differentiation patterns that appear in the callus; and for the first time in a 3D model healing was simulated beyond the reparative phase. In addition, this approach easily allows cell phenotype specific processes to be distinguished—such as the migration of motile cells (MSCs and fibroblasts) compared to non-motile cells. Despite some limitations the results demonstrate that models of this kind hold the potential to be used clinically to assess the options for treating fractures in individual patients.

ACKNOWLEDGMENTS

This work is funded by a Science Foundation Ireland Principal Investigator grant to P.J. Prendergast titled “Mechanobiological modeling for tissue engineering and medical device design.”

REFERENCES

- van der Meulen MCH, Huiskes R. 2002. Why mechanobiology? A survey article. *J Biomech* 35:401–414.
- Prendergast PJ. 2009. Papers in biomechanics and bioengineering. ScD Thesis, Dublin, Ireland: University of Dublin.
- Isaksson H, Donkelaar CCv, Huiskes R, et al. 2006. Corroboration of mechanoregulatory algorithms for tissue differentiation during fracture healing: comparison with in vivo results. *J Orthopaed Res* 24:898–907.
- Carter DR, Beaupré GS, Giorgi NJ, et al. 1998. Mechanobiology of skeletal regeneration. *Clin Orthopaed Relat Res* 355:S41–S55.
- Claes LE, Heigle CA. 1999. Magnitudes of local stress and strain along bony surfaces predict the course and type of fracture healing. *J Biomech* 32:255–266.
- Prendergast PJ, Huiskes R, Søballe K. 1997. Biophysical stimuli on cells during tissue differentiation at implant interfaces. *J Biomech* 30:539–548.
- Andreykiv A, Prendergast PJ, van Keulen F, et al. 2005. Bone ingrowth simulation for a concept glenoid component design. *J Biomech* 38:1023–1033.
- Lacroix D, Prendergast PJ. 2002. Three-dimensional simulation of fracture repair in the human tibia. *Comput Methods Biomed Eng* 5:369–376.

9. Andreykiv A, van Keulen F, Prendergast P. 2008. Simulation of fracture healing incorporating mechanoregulation of tissue differentiation and dispersal/proliferation of cells. *Biomech Model Mechanobiol* 7:443–461.
10. Hayward L, Morgan E. 2009. Assessment of a mechano-regulation theory of skeletal tissue differentiation in an in vivo model of mechanically induced cartilage formation. *Biomech Model Mechanobiol*. 8:447–455.
11. Kelly DJ, Prendergast PJ. 2006. Prediction of the optimal mechanical properties for a scaffold used in osteochondral defect repair. *Tissue Eng* 12:2509–2519.
12. Boccaccio A, Prendergast P, Pappalettere C, et al. 2008. Tissue differentiation and bone regeneration in an osteotomized mandible: a computational analysis of the latency period. *Med Biol Eng Comput* 46:283–298.
13. Geris L, Gerisch A, Sloten JV, et al. 2008. Angiogenesis in bone fracture healing: a bioregulatory model. *J Theor Biol* 251:137–158.
14. Khayyeri H, Checa S, Tagil M, et al. 2009. Corroboration of mechanobiological simulations of tissue differentiation in an in vivo bone chamber using a lattice-modeling approach. *J Orthopaed Res* 27:1659–1666.
15. Isaksson H, van Donkelaar CC, Huiskes R, et al. 2008. A mechano-regulatory bone-healing model incorporating cell-phenotype specific activity. *J Theor Biol* 252:230–246.
16. Pérez MA, Prendergast PJ. 2007. Random-walk models of cell dispersal included in mechanobiological simulations of tissue differentiation. *J Biomech* 40:2244–2253.
17. Huiskes R, Driel WDV, Prendergast PJ, et al. 1997. A biomechanical regulatory model for periprosthetic fibrous-tissue differentiation. *J Mater Sci Mater Med* V8:785–788.
18. Søballe K, Hansen ES, Rasmussen HB, et al. 1992. Tissue ingrowth into titanium and hydroxyapatite-coated implants during stable and unstable mechanical conditions. *J Orthopaed Res* 10:285–299.
19. Lacroix D, Prendergast PJ. 2002. A mechano-regulation model for tissue differentiation during fracture healing: analysis of gap size and loading. *J Biomech* 35:1163–1171.
20. Gerstenfeld LC, Cullinane DM, Barnes GL, et al. 2003. Fracture healing as a post-natal developmental process: molecular, spatial, and temporal aspects of its regulation. *J Cell Biochem* 88:873–884.
21. McMahon L, Reid A, Campbell V, et al. 2008. Regulatory effects of mechanical strain on the chondrogenic differentiation of MSCs in a collagen-GAG scaffold: experimental and computational analysis. *Ann Biomed Eng* 36:185–194.
22. Brighton CT, Schaffer JL, Shapiro DB, et al. 1991. Proliferation and macromolecular synthesis by rat calvarial bone cells grown in various oxygen tensions. *J Orthopaed Res* 9:847–854.
23. Bronner F, Farach-Carson MC, Rodan GA. 2003. Bone formation. London, England: Springer; 160 p.
24. Saltzman MW. 2004. Tissue engineering: engineering principles for the design of replacement organs and tissues, 1 ed. New York: Oxford University Press; 523 p.
25. Martin RB, Burr DB, Sharkey NA. 1998. Skeletal tissue mechanics. New York: Springer; 392 p.
26. Lacroix D, Prendergast P, Li G, et al. 2002. Biomechanical model to simulate tissue differentiation and bone regeneration: application to fracture healing. *Med Biol Eng Comput* 40:14–21.
27. Duda GN, Mandruzzato F, Heller M, et al. 2002. Mechanical conditions in the internal stabilization of proximal tibial defects. *Clin Biomech* 17:64–72.
28. Duda GN, Mandruzzato F, Heller M, et al. 2001. Mechanical boundary conditions of fracture healing: borderline indications in the treatment of unreamed tibial nailing. *J Biomech* 34:639–650.
29. Frost HM. 1986. Intermediary: organization of the skeleton. Boca Raton, Florida: Crc Press; 384 p.
30. Aranzulla PJ, Muckle DS, Cunningham JL. 1998. A portable monitoring system for measuring weight-bearing during tibial fracture healing. *Med Eng Phys* 20:543–548.
31. Duda GN, Eckert-Hubner K, Sokiranski R, et al. 1997. Analysis of inter-fragmentary movement as a function of musculoskeletal loading conditions in sheep. *J Biomech* 31:201–210.
32. Joslin CC, Eastaugh-Waring SJ, Hardy JRW, et al. 2008. Weight bearing after tibial fracture as a guide to healing. *Clin Biomech* 23:329–333.
33. Richardson JB, Cunningham JL, Goodship AE, et al. 1994. Measuring stiffness can define healing of tibial fractures. *J Bone Joint Surg* 76-B:389–394.
34. Gómez-Benito MJ, García-Aznar JM, Kuiper JH, et al. 2006. A 3D computational simulation of fracture callus formation: influence of the stiffness of the external fixator. *J Biomech Eng Trans ASME* 128:290–299.
35. Bailón-Plaza A, van Der Meulen MCH. 2001. A mathematical framework to study the effects of growth factor influences on fracture healing. *J Theor Biol* 212:191–209.
36. Bailón-Plaza A, van der Meulen MCH. 2003. Beneficial effects of moderate, early loading and adverse effects of delayed or excessive loading on bone healing. *J Biomech* 36:1069–1077.
37. Kearney EM, Prendergast PJ, Campbell VA. 2008. Mechanisms of strain-mediated mesenchymal stem cell apoptosis. *J Biomech Eng* 130:061004–061007.
38. Weyts FAA, Bosmans B, Niesing R, et al. 2003. Mechanical control of human osteoblast apoptosis and proliferation in relation to differentiation. *Calcif Tissue Int* 72:505–512.
39. Stops AJF, McMahon LA, O'Mahoney D, et al. 2008. A finite element prediction of strain on cells in a highly porous collagen-glycosaminoglycan scaffold. *J Biomech Eng* 130:061001.
40. Claes L, Augat P, Suger G, et al. 1997. Influence of size and stability of the osteotomy gap on the success of fracture healing. *J Orthopaed Res* 15:577–584.
41. Appeddu PA, Shur BD. 1994. Molecular analysis of cell-surface beta-1,4-galactosyltransferase function during cell-migration. *Proc Natl Acad Sci USA* 91:2095–2099.
42. Aubin JE, Liu F, Malaval L, et al. 1995. Osteoblast and chondroblast differentiation. *Bone* 17:S77–S83.
43. Bosnakovski D, Mizuno M, Kim G, et al. 2005. Isolation and multilineage differentiation of bovine bone marrow mesenchymal stem cells. *Cell Tissue Res* 319:243–253.